Structure and effective interactions in polymer nanocomposite melts: An integral equation theory study

Lei Zhao, Yi-Gui Li, Chongli Zhong,[a] and Jianguo Mi
Department of Chemical Engineering, Beijing University of Chemical Technology, Beijing 100029, China

(Received 16 December 2005; accepted 23 February 2006; published online 14 April 2006)

The polymer reference interaction site model from integral equation theory is used to investigate the structure and effective interactions in polymer nanocomposite melts where strong nanoparticle-monomer interactions are principally considered in this work. For finite particle volume fraction, the compromise for the interference between polymers and nanoparticles results in an optimum particle volume fraction for nanoparticle dispersion in polymer melts. At constant particle volume fraction, the effects of degree of polymerization become insignificant when it reaches a threshold value, below which quantitative effects on the organization states of polymer nanocomposite melts are found and help nanoparticles to well disperse in polymer. The aggregation of large nanoparticles decreases with the increase of the nanoparticle-monomer attraction strength. These observations may provide useful information for the development of new polymer materials. © *2006 American Institute of Physics*. [DOI: 10.1063/1.2187489]

I. INTRODUCTION

There has been much attention paid recently to the enhanced properties of polymers containing nanoscopic particles.[1–3] Compared to pure polymers and conventional composites, the polymer nanocomposites exhibit markedly improved mechanical[4–7] and viscoelastic[8–11] properties, and even biodegradability[6,12] because of their nanometer size and their large active surface. A detailed microscopic understanding of the structure and effective interactions in the polymer nanocomposites will greatly assist in developing strategies for rational design of nanomaterials.

Diverse simulation and theoretical approaches began to be employed to investigate elementary aspects of model polymer nanocomposites. Smith and co-workers employed molecular dynamics (MD) simulations to study the nanoparticle interactions in a melt of fully flexible bead-necklace chains, where all nonbonded interactions were modeled by Lennard-Jones (LJ) potentials.[13,14] Doxastakis *et al.* used a combined Monte Carlo simulation and integral equation theory to study the potential of mean force (PMF) in polymer nanocomposites.[15,16] In their simulations only a few nanoparticles were considered in the systems: one or two nanoparticles in Refs. 13–16, and five nanoparticles in Ref. 13 due to the equilibration difficulties and computational cost. Recently, Schweizer and co-workers employed the polymer reference interaction site model (PRISM) theory to study the structure, effective forces, and thermodynamics in dense polymer nanocomposite in the one- or two-nanoparticle limit.[17,18] Qualitative agreements were observed for the depletion forces between the PRISM theory and MD simulations. Various density functional theory (DFT) and "wall integral equation" investigations of dense polymer fluids confined between flat surfaces were performed by Yethiraj and Hall[19] and Yethiraj.[20] Patel and Egorov, on the other hand, developed and applied a new DFT to compute the PMF between two spherical nanoparticles in a concentrated solution of tangent fully flexible polymer chains.[21,22] To date, most existing theoretical works focused on the two nanoparticle problem and neglected the effects of particle volume fraction in the structural study of polymer nanocomposites; thus, the nanoparticle packing effect and interference between polymers and nanoparticles to achieve stable organization state in polymer nanocomposite melts remain challenging, which is the focus of this investigation.

In the present work, we employ the computationally convenient PRISM theory to investigate the structure and effective interactions in polymer nanocomposite melts where the nonbonded potentials for sites are modeled by LJ potentials. The purpose of this work is twofold: The first one is to compare the PRISM theory results with MD simulations to validate the accuracy of integral equation theory in describing the polymer nanocomposites. The second one is to study the effect of the particle volume fraction on the structure and effective interactions that is poorly understood experimentally and theoretically for the dense, meltlike conditions relevant to the polymer nanocomposites.

II. PRISM THEORY AND MODEL

Based on the reference interaction site model (RISM) theory proposed by Chandler and Andersen[23] and Chandler[24] for the various small rigid polyatomic liquids, Schweizer and Curro[25,26] developed the PRISM theory and used the theory to investigate various kinds of polymer systems such as polymer solutions[27,28] and colloid-polymer suspensions.[29–32] The principal output of the theory is the information about the intermolecular packing of the polymer as expressed through the intermolecular pair correlation function defined as

[a]Author to whom correspondence should be addressed. Electronic mail: zhongcl@mail.buct.edu.cn

$$\rho^2 g_{\alpha\gamma}(r) = \left\langle \sum_{i\neq j=1}^{M} \delta(r_i^{\alpha})\delta(r - r_j^{\gamma}) \right\rangle, \tag{1}$$

where M is the number of polymer molecules, $\rho = M/V$ is the number density of molecules, r_i^{α} specifies the position of site α on molecule i, and α and γ are interaction sites on different polymer molecules. By treating all sites on a molecule as statistically equivalent,[33] the matrix Ornstein-Zernike-type equations can be conveniently written in Fourier transform space as

$$\hat{h}_{ij}(k) = \hat{\omega}_l(k)\left[\hat{C}_{ij}(k)\hat{\omega}_j(k) + \sum_i \hat{C}_{il}(k)\rho_l\hat{h}_{lj}(k)\right], \tag{2}$$

where the caret denotes Fourier transformation with wave vector k, ρ_l is the site number density of species l, $h_{ij}(r) = g_{ij}(r) - 1$ is the intermolecular site-site total correlation function, $C_{ij}(r)$ is the corresponding intermolecular direct correlation function, and $\hat{\omega}_i(k)$ is the single molecule structure factor of species i. For nanoparticles the single molecule structure factor is unity $[\hat{\omega}_n(k) = 1]$. The polymer chain is treated as a freely joined chain (FJC) of N monomers, with site diameter σ and a rigid bond length $l = 1.269\sigma$. The choice of the rigid bond length reproduces the simulation R_g for polymer melts and matches the various results between a FJC hard core model in PRISM and a finite extensible nonlinear elastic (FENE) bead continuous model in MD.[34–36] Since the average bond length of the FENE chains (0.97σ) is approximately equal to the rigid bond length (σ) used in the MD simulations of polymer nanocomposites,[13,14] nearly the same models are employed between our PRISM and MD to investigate the polymer nanocomposite melts. The FJC structure factor is[35,37]

$$\hat{\omega}_p(k) = (1-f)^{-2}[1 - f^2 - 2N^{-1}f + 2N^{-1}f^{N+1}], \tag{3}$$

where $f = \sin(kl)/kl$. The nonideal conformational effects ignored by the FJC model are minor for the melt conditions of our present work. Equation (2) can be written as three coupled integral equations for polymer (p)-nanoparticle (n) system,

$$\hat{h}_{pp}(k) = \hat{\omega}_p^2(k)\hat{C}_{pp}(k) + \rho_n\hat{\omega}_p(k)\hat{C}_{pn}(k)\hat{h}_{np}(k) + \rho_p\hat{\omega}_p(k)\hat{C}_{pp}(k)\hat{h}_{pp}(k), \tag{4}$$

$$\hat{h}_{np}(k) = \hat{\omega}_p(k)\hat{C}_{np}(k) + \rho_n\hat{C}_{nn}(k)\hat{h}_{np}(k) + \rho_p\hat{C}_{np}(k)\hat{h}_{pp}(k), \tag{5}$$

$$\hat{h}_{nn}(k) = \hat{C}_{nn}(k) + \rho_n\hat{C}_{nn}(k)\hat{h}_{nn}(k) + \rho_p\hat{C}_{np}(k)\hat{h}_{pn}(k). \tag{6}$$

The potential of mean force between nanoparticles is given by

$$W_{nn}(r) = -\ln(g_{nn}(r))/\beta, \tag{7}$$

where $\beta = 1/k_BT$. The depletion forces between nanoparticles probe the derivative of the corresponding radial distribution functions,

$$f_{nn}(r) = \frac{\partial}{\partial r}\ln(g_{nn}(r))/\beta = -\frac{\partial}{\partial r}W_{nn}(r). \tag{8}$$

With the calculated $\hat{\omega}_i(k)$, closure approximations must be employed to uniquely determine $h_{ij}(r)$ and $C_{ij}(r)$. The site-site Percus-Yevick (PY) approximation[24,38] is adopted for the polymer-polymer and polymer-nanoparticle direct correlations,

$$C_{ij}(r) \cong g_{ij}(r)[1 - \exp(\beta U_{ij}(r))], \tag{9}$$

where $U_{ij}(r)$ is the total site-site interaction potential. The site-site PY closure has been shown to be accurate for pure polymers and polymer-nanoparticle correlations under dense melt conditions.[15,21,25,26] However, the use of PY closure for the nanoparticle-nanoparticle direct correlations results in unphysical negative nanoparticle-nanoparticle radial distribution functions in polymer nanocomposite melts.[17] Therefore, the hypernetted chain (HNC) closure[24,38] is used for the nanoparticle-nanoparticle direct correlations,

$$C_{nn}(r) \cong h_{nn}(r) - \ln g_{nn}(r) - \beta U_{nn}(r). \tag{10}$$

As discussed by Schweizer and co-workers,[17,18] the HNC closure is necessary to calculate the radial distribution functions between nanoparticles for the large size asymmetry situation and can qualitatively represent the simulation results for the depletion forces. The iterative Picard method is utilized to solve the integral equations.[38]

Regarding the nonbonded interactions $U_{ij}(r)$, the monomer-monomer, monomer-nanoparticle, and nanoparticle-nanoparticle interactions are all modeled via truncated and shifted LJ potentials,[13,14]

$$U_{ij}(r) = \infty, \quad r \leqslant R_{ij},$$

$$U_{ij}(r) = 4\varepsilon_{ij}\left[\left(\frac{\sigma}{r - R_{ij}}\right)^{12} - \left(\frac{\sigma}{r - R_{ij}}\right)^{6}\right], \quad R_{ij} < r < r_{ij}^{\mathrm{cut}},$$

$$U_{ij}(r) = 0, \quad r \geqslant r_{ij}^{\mathrm{cut}}, \tag{11}$$

which account for the excluded volume of the monomers and nanoparticles by offsetting the interaction range by R_{ij} ($R_{pp} = 0$ for polymer monomer-monomer interactions). R_{nn} is equal to $D - \sigma$ (here D is the diameter of the nanoparticle). All the interactions in this work are truncated and shifted so that the energy is zero at the separation $r = r_{ij}^{\mathrm{cut}}$. The monomer-nanoparticle and nanoparticle-nanoparticle interactions are taken into account from the surface of the nanoparticle, as illustrated schematically in Fig. 1(a).

The value of ε_{nn} is obtained so that the excess nanoparticle second virial coefficient B_2^{ex} is zero in the absence of the polymer,[39]

$$B_2^{\mathrm{ex}} = 2\pi\int_{R_{nn}}^{\infty}[1 - \exp(-\beta U_{nn}(r))]r^2dr = 0. \tag{12}$$

Accordingly, for the polymer nanocomposites, the nanoparticle second virial coefficient B_2 can be determined from the potential of mean force $W_{nn}(r)$ between nanoparticles given by

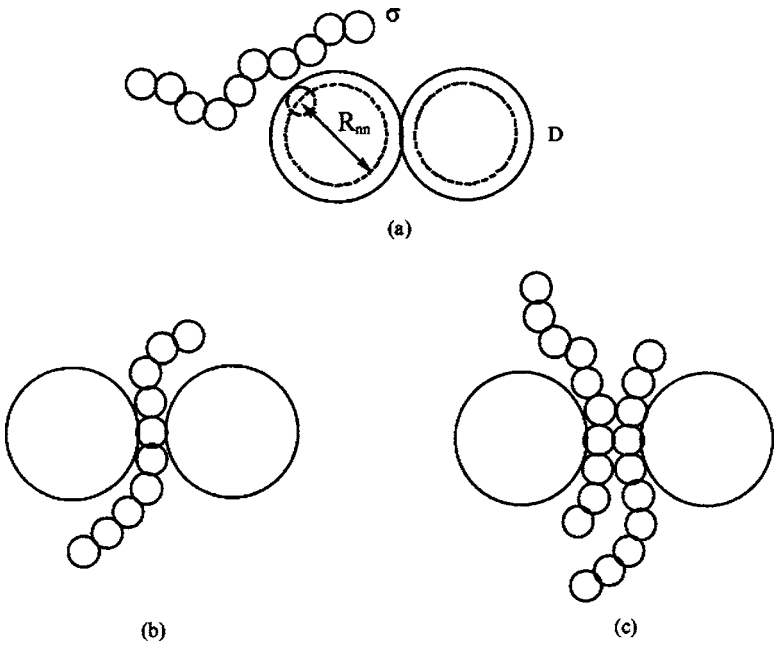

FIG. 1. Schematic illustration of three stable states of nanoparticle organization in polymer melts: (a) direct contact, (b) one polymer layer between nanoparticles, and (c) two polymer layers between nanoparticles.

$$B_2 = 2\pi \int_{R_{nn}}^{\infty} [1 - \exp(-\beta W_{nn}(r))] r^2 dr. \tag{13}$$

While knowledge of the B_2 alone is usually insufficient to allow prediction of phase behavior, it is a good indicator of the tendency of particles to aggregate or disperse within a solution. Positive values of $B_2^* = B_2/\sigma^3$ correspond to stable nanoparticle dispersions, while a negative value of B_2^* is indicative of a tendency for the nanoparticles to aggregate.[13,22]

III. COMPARISON OF PRISM THEORY AND SIMULATION

In order to ascertain the accuracy of the PRISM theory to describe the polymer nanocomposites, we compared our PRISM results to the MD simulation data reported by Smith and co-workers.[13,14] They employed MD simulations to investigate the structure and effective interactions on polymer nanocomposites consisting of one or two nanoparticles in polymer melts, which provided an excellent testing ground for PRISM theory treatments of the polymer nanocomposites. The conditions of the polymer melt were chosen to be the same as the MD simulations: $\rho_p \sigma^3 = 0.7$, $T^* = k_B T/\varepsilon_{pp} = 1.33$, and $N = 20$. We used the same model potential parameters as employed in the simulations: $\varepsilon_{nn} = 1.412\varepsilon_{pp}$, $\varepsilon_{np} = 2\varepsilon_{pp}$, $R_{nn} = 4\sigma$, $R_{np} = 2\sigma$, $r_{ij}^{\text{cut}} = R_{ij} + 2.5\sigma$.

In the infinitely dilute nanoparticle limit ($\rho_n \cong 0$), Eqs. (4)–(6) reduce to three uncoupled, sequentially solvable integral equations,[17,18]

$$\hat{h}_{pp}(k) = \hat{\omega}_p^2(k)\hat{C}_{pp}(k) + \rho_p \hat{\omega}_p(k)\hat{C}_{pp}(k)\hat{h}_{pp}(k), \tag{14}$$

$$\hat{h}_{np}(k) = \hat{\omega}_p(k)\hat{C}_{np}(k) + \rho_p \hat{C}_{np}(k)\hat{h}_{pp}(k), \tag{15}$$

$$\hat{h}_{nn}(k) = \hat{C}_{nn}(k) + \rho_p \hat{C}_{np}^2(k)(\hat{\omega}_p(k) + \rho_p \hat{h}_{pp}(k)). \tag{16}$$

We first calculated the nanoparticle-monomer radial distribution function $g_{np}(r)$ of one nanoparticle dissolved in a polymer melt using Eqs. (14) and (15), which are independent of the closure for the nanoparticle-nanoparticle direct correlations. The corresponding results obtained from the PRISM theory are shown in Fig. 2, where the simulation data[14] for the nanoparticle-monomer radial distribution function were also reproduced for comparison. As can be seen from Fig. 2, the PRISM theory results are in good agreement with the simulation results. Both the theory and simulation results exhibit clear oscillatory behavior; the first peak is located at $r/\sigma \sim 3.0$ and subsequent peaks are at integer multiples of monomer diameter σ, indicating monomer layers formed around the nanoparticles.

We then compared the PRISM theory and MD simulation results for the potential of mean force between two nanoparticles in Fig. 3. It can be seen that the PRISM theory results for the PMF are in good agreement with simulation.[13] The possible reason leading to the quantitative differences between theory and simulation is the use of atomic closures within the PRISM framework.

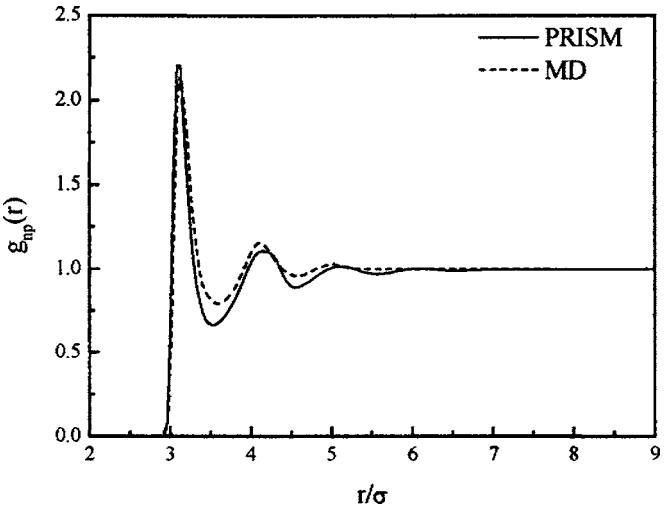

FIG. 2. Nanoparticle-monomer radial distribution function $g_{np}(r)$ of one-nanoparticle limit in polymer melts.

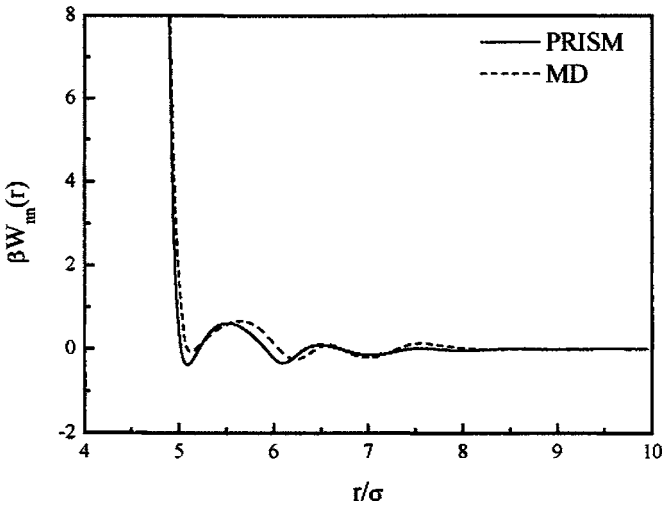

FIG. 3. Potential of mean force between two nanoparticles.

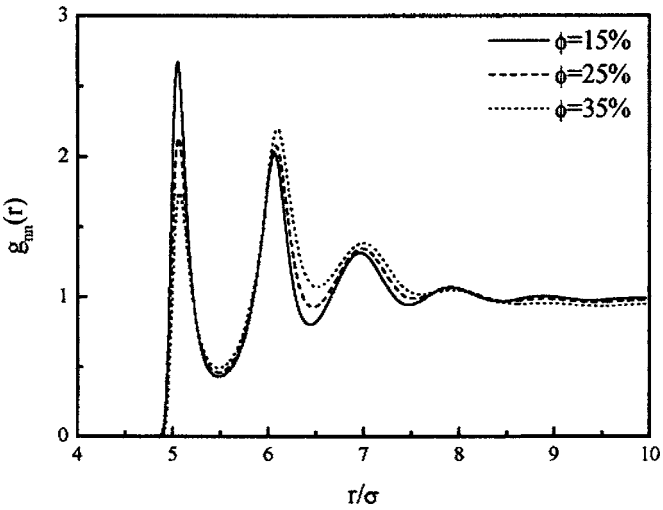

FIG. 4. Nanoparticle-nanoparticle radial distribution functions for different particle volume fractions.

It can be seen from Figs. 2 and 3 that the PRISM theory is reliable to describe the structure and effective interactions in polymer nanocomposite melts with one- or two-nanoparticle limit. It cannot only reproduce the main features of the simulation results, but also can obtain nearly quantitative agreement with the MD simulations, stimulating us to extend the PRISM theory to predict the properties of the polymer nanocomposites where the particle volume fractions are nonzero.

IV. PREDICTIONS OF THE POLYMER NANOCOMPOSITE FOR NONZERO PARTICLE VOLUME FRACTIONS

In this section we predicted the structure and effective interactions in the polymer nanocomposite melts with nonzero particle volume fractions, which have been rarely studied from both theory and simulation. We examine the systems with very attractive nanoparticle-monomer interactions due to the numerical limitations in PRISM theory based on the HNC closure. For example, it can preclude convergence at finite particle volume fraction for the systems with weak nanoparticle-monomer interactions where nanoparticles aggregate. The roles of the particle volume fraction, degree of polymerization, and nanoparticle-monomer size ratio were systematically investigated in this work.

We assumed that the number densities of the monomers were decreased in mixture with the addition of nanoparticles and the total packing fractions of the mixtures were fixed as the meltlike packing fraction of 0.5 in all our calculations.[26] The particle volume fraction ϕ is expressed as follows:

$$\phi = \frac{\rho_n \alpha^3}{\rho_p + \rho_n \alpha^3}, \tag{17}$$

where α is the nanoparticle-monomer size ratio D/σ, and ρ_p and ρ_n are the number density of polymer monomers and nanoparticles after mixing, respectively. In this investigation the dimensionless temperature is taken as $T^*=1.33$. Unless stated otherwise, the diameter of nanoparticle is $D=5\sigma$, the chain length is $N=80$, and the nonbonded potential parameters are the same as described in Sec. III.

A. Effects of the particle volume fraction

The most important quantity that PRISM is able to calculate is the radial distribution function $g(r)$ completely describing the packing structure of polymers and nanoparticles in the mixture. Many important thermodynamic properties of interest can be computed from it with the interaction potential $U(r)$. Therefore, we firstly calculated the radial distribution functions between nanoparticles $g_{nn}(r)$ to investigate the effects of the particle volume fraction on the polymer nanocomposites. Three different particle volume fractions were considered in this work as examples, $\phi=15\%$, 25%, and 35%, which are much larger than those studied by Smith and co-workers[13,14] (3% for two nanoparticles and 7% for five nanoparticles in polymer melts). The calculated results $g_{nn}(r)$ with three different particle volume fractions are depicted in Fig. 4. Obvious oscillatory behaviors were observed from Fig. 4 for the radial distribution functions between nanoparticles. There exist three evident peaks at $r/\sigma \sim 5.0$, 6.0, and 7.0, representing the three different stable states of organization between nanoparticles as illustrated schematically in Fig. 1: (a) direct contact, (b) one polymer layer between nanoparticles, and (c) two polymer layers between nanoparticles. With the increase of the particle volume fraction, the interference between the largely decrease of polymer number density and slowly increase of nanoparticle number density leads to the decrease of the intensity of the first peak.

The potential of mean force represents the potential between nanoparticles considering all the nanoparticles and polymers induced in the system and can exhibit the different states of organization for the polymer nanocomposite melts. The PMF values calculated from the PRISM theory for various particle volume fractions are given in Fig. 5. One can see that the nanoparticles preferred well-defined locations such as the attractive minima in the PMF, indicating that the nanoparticles are favorably located at $r/\sigma \sim 5.0$, 6.0, and 7.0, which is consistent with the behavior of the radial distribution functions between nanoparticles, as shown in Fig. 4. The attractive minima for PMF value did not achieve to the value of $5k_BT$ which is generally adequate to induce aggregation of

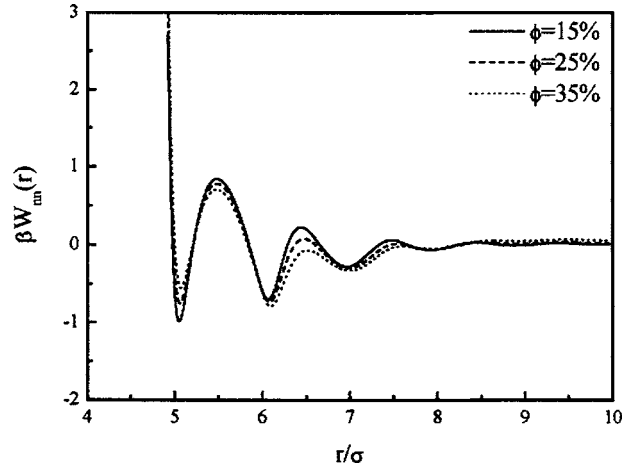

FIG. 5. Potentials of mean force for different particle volume fractions.

particles according to the knowledge of colloid science.[17] The depletion forces between nanoparticles calculated from Eq. (8) are given in Fig. 6, showing similar tendency to the PMF by increasing particle volume fractions.

Following Eq. (13), the second virial coefficient B_2^* calculated for different particle volume fractions are listed in Table I. It can be concluded that in the situation of strong nanoparticle-monomer attractions there perhaps exist an optimum particle volume fraction for the nanoparticles to disperse in polymer melts because a maximum B_2^* value was observed in the table, probably caused by the compromise for the interference between polymers and nanoparticles.

B. Effects of degree of polymerization

The degree of polymerization (N) is expected to have effects on the mode of organization in polymer nanocomposite melts, which can help us to understand the possibility to achieve miscibility and good particle dispersion in real polymer nanocomposites. To explore the role of degree of polymerization in the polymer nanocomposites with nonzero particle volume fractions, we computed four N values with the particle volume fractions $\phi=25\%$ as instances: $N=10$, 20, 80, and 200. The results predicted from the PRISM theory

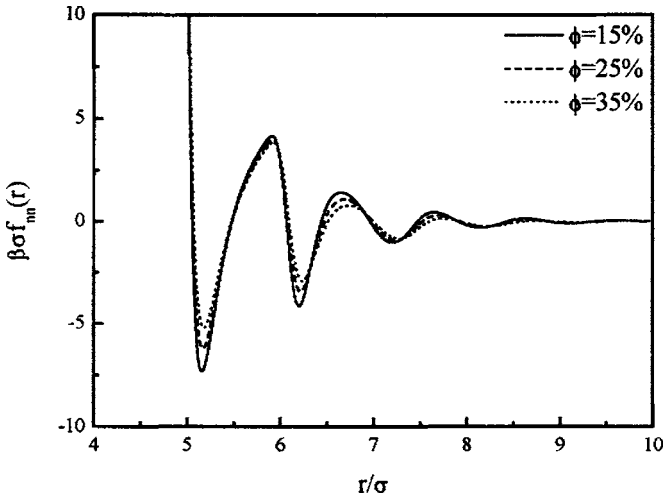

FIG. 6. Depletion forces for different particle volume fractions.

TABLE I. Second virial coefficients for different particle volume fractions.

ϕ (%)	N	α	$\varepsilon_{np}/\varepsilon_{pp}$	B_2^*
10	80	5	2	131
15	80	5	2	139
20	80	5	2	143
25	80	5	2	145
30	80	5	2	144
35	80	5	2	140
40	80	5	2	136

for the radial distribution functions between nanoparticles are shown in Fig. 7. An interesting phenomenon was observed from Fig. 7 that the intensity of the first peak in the $g_{nn}(r)$ curves is largely decreased with the increase of the degree of polymerization. More nanoparticles are packing in the state of direct contact than that of one and two polymer layers between nanoparticles for short chain length, illustrated by the dominant peak at $r/\sigma\sim5.0$ and the relative weak peaks at $r/\sigma\sim6.0$ and 7.0. With the increasing of N, more nanoparticles are separated or wrapped by the polymers, leading to the large decrease of the intensity of the first peak. It can be deduced from Fig. 7 that the effects on the $g_{nn}(r)$ curves become very small when N reaches a threshold value in the case of strong nanoparticle-monomer attractions. Below this threshold value, the degree of polymerization quantitatively affects on the organization states of polymer nanocomposite melt for constant particle volume fractions, which helps nanoparticles to well disperse in polymer melts.

Figures 8 and 9 show the calculated PMF and depletion force for different degrees of polymerization using the PRISM theory, respectively. The attractive minima in the PMF and depletion force all became deeper with the decreasing of N, while the repulsive maxima slightly increased with the decrease of N. The differences between the curves of $N=80$ and 200 are very small, resulting in the conclusion that the effects of N on the potential of mean force and depletion force are insignificant when the degree of polymerization

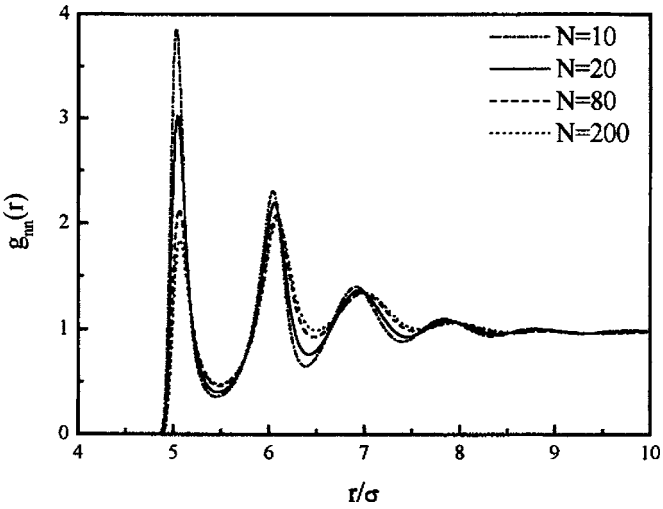

FIG. 7. Nanoparticle-nanoparticle radial distribution functions for different degrees of polymerization with $\phi=25\%$.

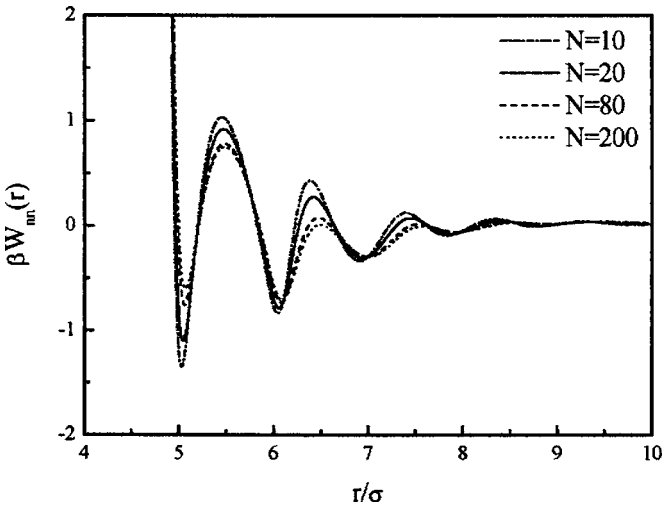

FIG. 8. Potentials of mean force for different degrees of polymerization with $\phi=25\%$.

reaches a threshold value. This is consistent with the conclusion obtained from the radial distribution functions between nanoparticles.

The second virial coefficient is the integration over the potential of mean force that captures the net effect of the competition between attractive and repulsive regions of PMF. Therefore, it is used to evaluate the effects of N on the nanoparticle dispersion in polymer melts. The second virial coefficient B_2^* results for different degrees of polymerization with $\phi=25\%$ are depicted in Fig. 10. Our results are different compared with those from Smith *et al.*[13] who found that the tendency to disperse (positive B_2^*) is independent of chain length for $\varepsilon_{np}/\varepsilon_{pp}=2$ even in short chain ($N\leqslant 20$). From Fig. 10, we can see that the B_2^* value is independent of the degree of polymerization until it is larger than a certain value. It can be explained that the effects of N on the potential of mean force are insignificant when the degree of polymerization reaches a threshold value. It seems that the long chains cannot give a more stable dispersion for nanoparticles compared with the short chains as the B_2^* decreases with the increase of N before the threshold value.

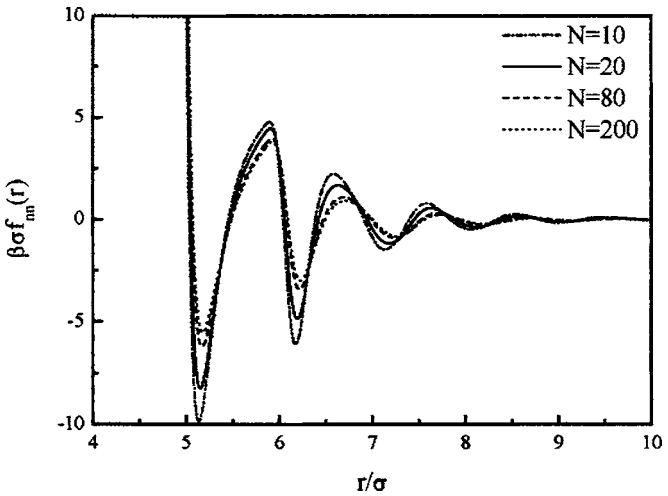

FIG. 9. Depletion forces for different degrees of polymerization with $\phi=25\%$.

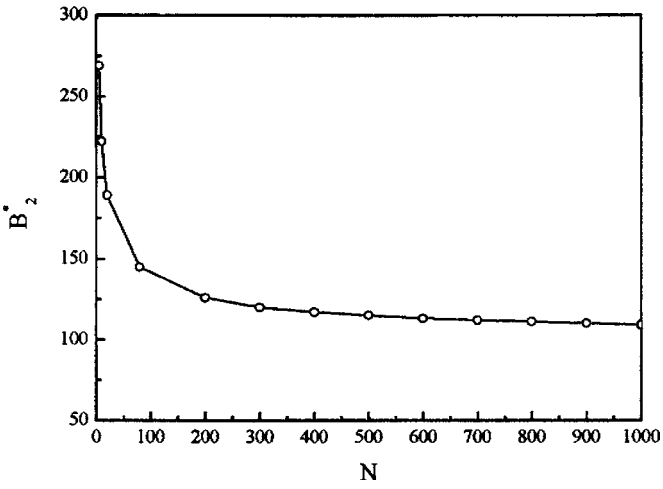

FIG. 10. Second virial coefficients for different degrees of polymerization with $\phi=25\%$.

C. Effects of nanoparticle size

Furthermore, the effects of the nanoparticle size on the polymer nanocomposites were studied. In this work, three nanoparticle-monomer size ratios ($\alpha=5$, 9, and 17) were considered, and the corresponding ε_{nn} values were obtained as $\varepsilon_{nn}/\varepsilon_{pp}=1.412$, 1.615, and 1.71 utilizing $B_2^{ex}=0$ [see Eq. (12)]. The B_2^* values calculated from the PRISM theory are listed in Table II. As can be seen from Table II, in the infinitely dilute nanoparticle limit systems ($\phi=0$), three large negative B_2^* values were obtained for relatively weak nanoparticle-monomer attractions, indicating that a strong tendency for the nanoparticles to aggregate in a roughly spherical compact cluster. Similar tendency can be illustrated by the strong intensity of the first peak in the curves of $g_{nn}(r)$, which are not shown in this paper. In these three systems with relatively weak nanoparticle-monomer attractions, PRISM theory based on HNC closure precludes convergence even at very small particle volume fraction. It also can be seen from Table II that the aggregation for large nanoparticles can be overcome with the increase of the nanoparticle-monomer attraction strength ε_{np}. Therefore, we fixed the nanoparticle-monomer attraction strength at $\varepsilon_{np}/\varepsilon_{pp}=3.0$ to investigate the effect of the nanoparticle size on the polymer nanocomposites, where the nanoparticles are well dispersed in the polymer melts.

The radial distribution functions between nanoparticles for different particle sizes with $\phi=10\%$ are shown in Fig. 11 where interparticle distances are discussed in terms of the

TABLE II. Second virial coefficients for different nanoparticle-monomer size ratios.

ϕ (%)	N	α	$\varepsilon_{np}/\varepsilon_{pp}$	B_2^*
0	80	5	1	−18 460
0	80	9	2	−2 907
0	80	17	2	−1 482 543
10	80	5	3	288
10	80	9	3	1 447
10	80	17	3	18 579

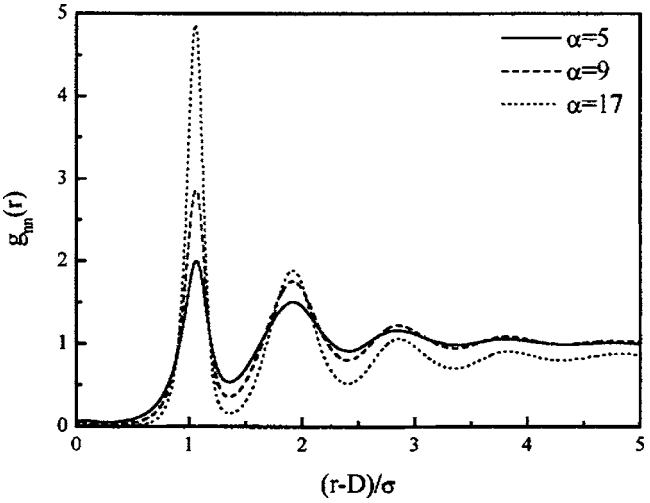

FIG. 11. Nanoparticle-nanoparticle radial distribution functions for different nanoparticle-monomer size ratios with $\phi=10\%$.

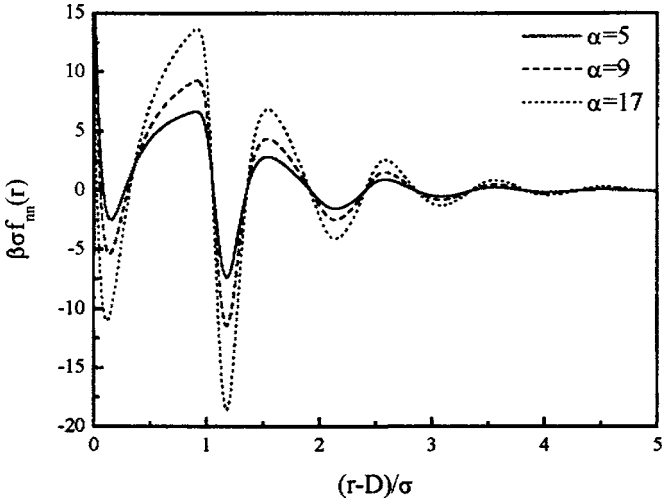

FIG. 13. Depletion forces for different nanoparticle-monomer size ratios with $\phi=10\%$.

reduced filler surface-to-surface separation $(r-D)/\sigma$. There are two evident peaks at $(r-D)/\sigma\sim 1.0$ and 2.0, revealing that one or two polymer layers are formed between the nanoparticles at least as the chains adsorb onto the surface of the nanoparticle due to the large ε_{np}. Most particles are wrapped by the polymer monomers leading to the absence of nanoparticles at contact interparticle separation. This interprets the good dispersion of nanoparticles in the polymer melts for large ε_{np}. As can be seen from Fig. 11, the intensity of the two peaks at $(r-D)/\sigma\sim 1.0$ and 2.0 increases with the increasing of the nanoparticle-monomer size ratio. As expected, the specific surface increases with the decrease of the particle size at constant particle volume fractions, leading to more polymer monomers adsorb on the surface of nanoparticle and then squeeze out the other nanoparticles around.

The PMF values calculated from the PRISM theory for different nanoparticle-monomer size ratios are given in Fig. 12. The first large repulsive maximum in the PMF curves increases greatly with the increase of nanoparticle size that prevent the nanoparticle to move to the other nanoparticles. The global attractive minima appear at about $(r-D)/\sigma=1.0$ with the distance between the surfaces of nanoparticles. The attractive minima in the PMF become deeper with the increase of the particle size, demonstrating that the larger nanoparticles are likely to be located at the attractive minima of PMF. The depletion forces calculated from the PRISM are displayed in Fig. 13. Similar to the curves of PMF, increasingly larger repulsive maxima appear with the increase of particle size, preventing the nanoparticle from moving to the other nanoparticles. These repulsive maxima are expected to promote the dispersion of nanoparticles in polymer melts.

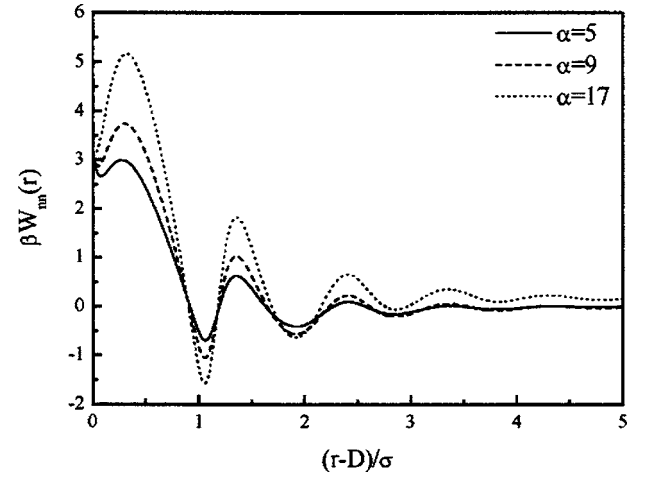

FIG. 12. Potentials of mean force for different nanoparticle-monomer size ratios with $\phi=10\%$.

V. CONCLUSIONS

The PRISM integral equation theory was used to investigate the structure and effective interactions in polymer nanocomposite melts, where the strong nanoparticle-monomer interactions were principally considered in this work. The calculated results for the radial distribution function and potential of mean force show that the PRISM based on HNC closure for nanoparticle-nanoparticle direct correlations agrees well with molecular dynamics simulations for the systems with one and two nanoparticles. Besides the radial distribution function, potential of mean force, and depletion force, we also used the second virial coefficient as an indicator of dispersion or aggregation of the nanoparticles. When extending to the finite particle volume fraction, the compromise for the interference between polymers and nanoparticles results in a maximum value of B_2^* indicating an optimum particle volume fraction for nanoparticle dispersion in polymer melts with strong nanoparticle-monomer attractions. For constant particle volume fraction, the effects of degree of polymerization become insignificant when it reaches a threshold value, below which quantitative effects on the organization states of polymer nanocomposite melts were found and help nanoparticles to well disperse in polymer. In addition, this work found that the aggregation of large nanoparticles decreases with the increase of the nanoparticle-monomer attraction strength. All these observations give molecular-level details of the underlying mecha-

nisms, providing useful information for the future design of new nanocomposite materials with tailored properties.

ACKNOWLEDGMENT

The financial support of the NSFC (20476003 and 20576006) and the Specialized Research Fund for the Doctoral Program of Higher Education of China (20040010002) is greatly appreciated.

[1] E. Harth, B. V. Horn, V. Y. Lee, D. S. Germack, C. P. Gonzales, R. D. Miller, and C. J. Hawker, J. Am. Chem. Soc. **124**, 8653 (2002).
[2] M. E. Mackay, T. T. Dao, A. Tuteja, D. L. Ho, B. V. Horn, H. C. Kim, and C. J. Hawker, Nat. Mater. **2**, 762 (2003).
[3] Y. Lin, A. Boker, J. He *et al.*, Nature (London) **434**, 55 (2005).
[4] H.-J. Gläsel, E. Hartmann, R. Mehnert, D. Hirsch, R. Böttcher, and J. Hormes, Nucl. Instrum. Methods Phys. Res. B **151**, 200 (1999).
[5] H.-J. Gläsel, E. Hartmann, D. Hirsch, R. Böttcher, D. Michel, J. Hormes, and H. Rumpf, J. Mater. Sci. **43**, 2319 (1999).
[6] A. Dufresne, J. Y. Cavaille, and W. Helbert, Macromolecules **29**, 7624 (1996).
[7] A. Dufresne, J. Y. Cavaille, and W. Helbert, Polym. Compos. **17**, 604 (1996).
[8] F. Bauer, H. Ernst, U. Decker, M. Findeisen, H.-J. Gläsel, H. Langguth, E. Hartmann, R. Mehnert, and C. Peuker, Macromol. Chem. Phys. **201**, 2654 (2000).
[9] H.-J. Gläsel, F. Bauer, H. Ernst, M. Findeisen, E. Hartmann, H. Langguth, R. Mehnert, and R. Schubert, Macromol. Chem. Phys. **201**, 2765 (2000).
[10] F. Bauer, V. Sauerland, H.-J. Gläsel, H. Ernst, M. Findeisen, E. Hartmann, H. Langguth, B. Marquardt, and R. Mehnert, Macromol. Mater. Eng. **287**, 546 (2002).
[11] F. Bauer, H. Ernst, D. Hirsch, S. Naumov, M. Pelzing, V. Sauerland, and R. Mehnert, Macromol. Chem. Phys. **205**, 1587 (2004).
[12] C. M. Niemeyer, Angew. Chem., Int. Ed. **40**, 4128 (2001).
[13] J. S. Smith, D. Bedrov, and G. D. Smith, Compos. Sci. Technol. **63**, 1599 (2003).
[14] D. Bedrov, G. D. Smith, and J. S. Smith, J. Chem. Phys. **119**, 10438 (2003).
[15] M. Doxastakis, Y. L. Chen, O. Guzman, and J. J. de Pablo, J. Chem. Phys. **120**, 9335 (2004).
[16] M. Doxastakis, Y. L. Chen, and J. J. de Pablo, J. Chem. Phys. **123**, 034901 (2005).
[17] J. B. Hooper, K. S. Schweizer, T. G. Desai, R. Koshy, and P. Keblinski, J. Chem. Phys. **121**, 6986 (2004).
[18] J. B. Hooper and K. S. Schweizer, Macromolecules **38**, 8858 (2005).
[19] A. Yethiraj and C. K. Hall, J. Chem. Phys. **95**, 3749 (1991).
[20] A. Yethiraj, Adv. Chem. Phys. **121**, 89 (2002).
[21] N. Patel and S. A. Egorov, J. Chem. Phys. **121**, 4987 (2004).
[22] N. Patel and S. A. Egorov, J. Chem. Phys. **123**, 144916 (2005).
[23] D. Chandler and H. C. Andersen, J. Chem. Phys. **57**, 1930 (1972).
[24] D. Chandler, in *Studies in Statistical Mechanics VIII*, edited by E. W. Montroll and J. L. Lebowitz (North-Holland, Amsterdam, 1982), p. 274.
[25] K. S. Schweizer and J. G. Curro, Adv. Polym. Sci. **116**, 321 (1994).
[26] K. S. Schweizer and J. G. Curro, Adv. Chem. Phys. **98**, 1 (1997).
[27] S. Mendez, J. G. Curro, M. Pütz, D. Bedrov, and G. D. Smith, J. Chem. Phys. **115**, 5669 (2001).
[28] S. Mendez and J. G. Curro, Macromolecules **37**, 1980 (2004).
[29] A. Yethiraj, C. K. Hall, and R. Dickman, J. Colloid Interface Sci. **151**, 102 (1992).
[30] M. Fuchs and K. S. Schweizer, Europhys. Lett. **51**, 621 (2000).
[31] M. Fuchs and K. S. Schweizer, Phys. Rev. E **64**, 021514 (2001).
[32] M. Fuchs and K. S. Schweizer, J. Phys.: Condens. Matter **14**, R239 (2002).
[33] J. G. Curro and K. S. Schweizer, J. Chem. Phys. **87**, 1842 (1987).
[34] K. Kremer and G. S. Grest, J. Chem. Phys. **92**, 5057 (1990).
[35] J. G. Curro, K. S. Schweizer, G. S. Grest, and K. Kremer, J. Chem. Phys. **91**, 1357 (1989).
[36] R. Koshy, T. G. Desai, P. Keblinski, J. Hooper, and K. S. Schweizer, J. Chem. Phys. **119**, 7599 (2003).
[37] M. Doi and S. F. Edwards, *Theory of Polymer Dynamics* (Oxford University Press, New York, 1986).
[38] J. P. Hansen and I. R. McDonald, *Theory of Simple Liquids*, 2nd ed. (Academic, London, 1986).
[39] D. McQuarrie, *Statistical Mechanics* (Harper & Row, New York, 1976).